Journal of Energy Storage 19 (2018) 379–392

Contents lists available at ScienceDirect

Journal of Energy Storage

journal homepage: www.elsevier.com/locate/est

Performance response of packed-bed thermal storage to cycle duration perturbations

Joshua D. McTigue[a,*], Christos N. Markides[b], Alexander J. White[c]

[a] National Renewable Energy Laboratory, 15013 Denver West Parkway, Golden, CO 80401, USA
[b] Clean Energy Processes (CEP) Laboratory, Department of Chemical Engineering, Imperial College London, London SW7 2AZ, UK
[c] Cambridge University Engineering Department, Trumpington Street, Cambridge CB2 1PZ, UK

ARTICLE INFO

Keywords:
Thermal energy storage
Thermocline
Packed bed
Exergy analysis
Heat transfer
Partial-charge

ABSTRACT

Packed-bed thermal stores are integral components in numerous bulk electricity storage systems and may also be integrated into renewable generation and process heat systems. In such applications, the store may undergo charging and discharging periods of irregular durations. Previous work has typically concentrated on the initial charging cycles, or on steady-state cyclic operation. Understanding the impact of unpredictable charging periods on the storage behavior is necessary to improve design and operation. In this article, the influence of the cycle duration (or 'partial-charge' cycles) on the performance of such thermal stores is investigated. The response to perturbations is explained and provides a framework for understanding the response to realistic load cycles.

The packed beds considered here have a rock filler material and air as the heat transfer fluid. The thermodynamic model is based on a modified form of the Schumann equations. Major sources of exergy loss are described, and the various irreversibility generating mechanisms are quantified.

It is known that repeated charge-discharge cycles lead to steady-state behavior, which exhibits a trade-off between round-trip efficiency and stored exergy, and the underlying reasons for this are described. The steady state is then perturbed by cycles with a different duration. Short duration perturbations lead to a transient decrease in exergy losses, while longer perturbations increase it. The magnitude of the change in losses is related to the perturbation size and initial cycle period, but changes of 1–10 % are typical. The perturbations also affect the time to return to a steady-state, which may take up to 50 cycles. Segmenting the packed bed into layers reduces the effect of the perturbations, particularly short durations.

Operational guidelines are developed, and it is found that packed beds are more resilient to changes in available energy if the store is not suddenly over-charged (i.e. longer perturbations), and if the steady-state cycle duration is relatively long. Furthermore, using the gas exit temperature to control cycle duration reduces the impact of perturbations on the performance, and reduces the time to return to steady-state operation.

1. Introduction

Packed beds have been proposed for a variety of thermal energy storage applications, including bulk electricity storage systems such as advanced-adiabatic compressed-air energy storage (AA-CAES) [1,2], liquid-air energy storage (LAES) [3], and pumped-thermal (or, pumped-heat elsewhere in the literature) electricity storage (PTES/PHES) [4–6]. They have also been suggested for use in other systems that involve thermal processes, such as concentrating solar power, geothermal energy, and process heat. Packed beds are potentially more compact and cost-effective than conventional storage systems, such as two-tank liquid stores. Depending on the heat transfer fluid and storage media, they also tend to use more abundant and locally sourced, lower cost, environmentally-benign, and non-reactive materials than other storage technologies.

Typically, a packed bed is a storage vessel filled with a solid packing medium (the "filler") such as pebbles or gravel, as illustrated in Fig. 1. Energy is transferred to the solid by means of the heat transfer fluid (HTF), which may also be the working fluid in whatever system the packed bed is part of. Many packed bed designs exist in the literature, with variations in the geometry, storage medium, and HTF. Stores are typically cylindrical with the HTF travelling axially. Hot fluid usually enters at the top and leaves at the bottom in order to avoid buoyancy-driven flows. The filler material is generally a solid such as alumina, ceramic, or crushed rock. Such packed beds are classified as 'sensible heat' storage since energy is stored by virtue of the temperature change

* Corresponding author.
E-mail address: JoshuaDominic.McTigue@nrel.gov (J.D. McTigue).

https://doi.org/10.1016/j.est.2018.08.016
Received 13 July 2018; Received in revised form 15 August 2018; Accepted 20 August 2018
Available online 01 September 2018
2352-152X/ Published by Elsevier Ltd. This is an open access article under the CC BY license (http://creativecommons.org/licenses/BY/4.0/).

Nomenclature

Abbreviations

AA-CAES	Advanced-adiabatic compressed-air energy storage
CSP	Concentrating solar power
HTF	Heat transfer fluid
LAES	Liquid-air energy storage
PTES/PHES	Pumped-thermal electricity storage/pumped-heat electricity storage

Roman symbols

A	Cross-sectional area (m^2)
A_w	Wall surface area (m^2)

Roman symbols

B	Exergy (J)
C_f	Coefficient of friction
c_p	Specific heat capacity of gas or solid (J/kg K)
$\mathscr{C}$	Unsteady gas term (K/m)
d_p	Particle diameter (m)
D	Diameter (m)
E	Energy capacity of packed bed (Wh_{th})
G	Mass flow rate per unit area (kg/s m^2)
k_{eff}	Effective conductivity (W/m K)
L	Length (m)
ℓ	Packed bed length scale (m)
$\dot{m}$	Mass flow rate (kg/s)
p	Pressure bar
$\dot{P}$	Power output of packed bed (W_{th})
Re	Reynolds number
S_{irr}	Entropy (J/K)
S_v	Particle surface area to volume ratio (m^{-1})
St	Stanton number
t	Time (s)
t_{chg}	Charging duration (s)
t_N	Nominal charging time (s)
T	Temperature (°C, K)
U_w	Overall heat transfer coefficient (W/m^2 K)
V_f	Thermal front velocity (m/s)
x	Distance (m)

Greek symbols

α	Packed bed diffusivity (m^2/s)
β	Reduced availability (K)
γ	Ratio of gas specific heat capacities
ε	Packed bed void fraction
ρ	Density (kg/m^3)
ζ	Exergy loss coefficient
ϕ	Packed bed heat leakage time constant (s^{-1})
Π	Dimensionless cycle duration, t_{chg}/t_N
η_{RT}	Round-trip efficiency (%)
θ	Normalized exit temperature
τ	Packed bed time scale (s)

Superscripts and subscripts

c, h	Cold, hot
g, s	Gas, solid
o	Steady-state value
chg, dis	Charging, discharging
in, out	Inlet, exit
x	Exit temperature

of the filler. Encapsulated phase change materials may also be used, however, thereby creating a latent heat storage system [7], but this increases the cost and complexity. HTFs may be gases, such as air [8,9] or argon [10], or liquids, such as thermal oils [11] or molten salts [12]. This article considers a cylindrical store, filled with particles of magnetite (Fe_3O_4) and uses air as the heat transfer fluid. The rationale and methodology follows earlier publications of the present authors [10,13–15], and is summarized below.

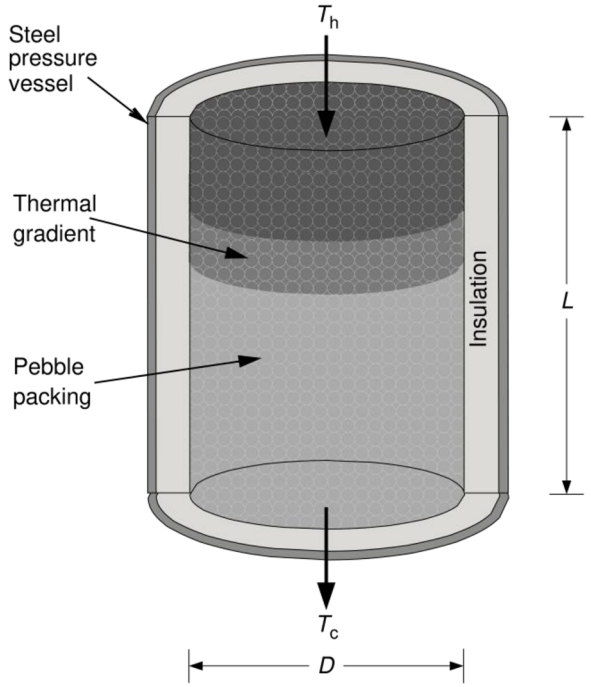


Fig. 1. Schematic of a packed-bed thermal store. Hot gas enters at the top at temperature T_h and exits from the bottom at temperature T_c.

1.1. Packed bed design considerations

Several technical challenges must be resolved before packed-bed thermal stores are likely to become commercially widespread. Careful design is required to mitigate the trade-off between heat transfer losses and frictional pressure losses – these being the exergy loss components that dominate thermal store behavior [13]. Understanding these loss mechanisms, and the influence of design and operational parameters upon them is necessary to improve system performance. Detailed analysis of packed beds has led to several novel designs that optimize storage efficiencies. For instance, the stores may be segmented into layers [15,16] in order to mitigate the inherent conflict between pressure loss and high heat transfer surface. These layers may consist of different materials [17]. Other geometries that have been proposed include conical stores [18,19], and radial-flow stores [10,20] both of which reduce pressure losses by increasing the flow area. Conical stores can also reduce the negative impacts of 'thermal ratcheting' which is caused by thermal expansion of particles and which may damage the containment vessel and packing. Radial-flow stores were found to have similar performance to axial-flow stores, but the additional volume required for bypass flows leads to increased capital costs [10].

Efficient operation of packed beds requires effective control of the thermal front. The thermal front (or thermocline) is the region of the bed where heat transfer between the fluid and solid occurs, and is characterized by significant temperature gradients. The thermal front length depends on the design and operation parameters, and it also changes throughout charge and discharge. The length and shape of the thermal front influences the efficiency and energy density of the packed bed, as will be discussed further below.

The progression of the thermal front along the packed bed eventually leads to variations in the exit temperature of the fluid. Any system that the packed bed is part of may need to limit the maximum change in this temperature. For instance, in a concentrating solar power (CSP) plant, if the fluid returns to the solar field at an increased temperature then it may be heated to even higher temperatures in the solar receivers. The maximum operating temperature of the HTF therefore imposes constraints on the packed bed exit temperature [21]. This effectively means that the packed bed cannot be fully charged and thus needs to be oversized to provide the required energy storage.

Researchers have sought to stabilize exit temperatures by various means, including incorporating phase change materials into the store [7,22,23], and rejecting heat from the exit flow to the environment. Similarly, some inlet flow can be bypassed around the store during discharge with this cooler flow used to 'attemporize' the hot exit flow down to some defined value. As the thermal front progresses out of the store, the exit temperature drops during discharge, so the fraction of bypassed flow is decreased to maintain a constant exit temperature. The mixing processes means, however, that the full exergetic potential of the store is not exploited.

1.2. Influence of variable charge-discharge durations on packed bed behavior

Much of the literature on packed beds concentrates on either 'single-blow' (i.e. a single charge-discharge process) or 'cyclic operation'. A number of studies have been presented on the effects of inlet temperature variation on single-blow operation, including those presented in [24,25] and the experimentally-validated transient response analysis of Beasley and Clark [26]. Other authors have previously studied variations in inlet temperatures [24,25]. Esence et al. [27] investigated thermocline development during the first charge cycle and described the effect of pre-existing thermal profiles in the packed bed.

Under cyclic operation the store is repeatedly charged and discharged until steady-state periodic operation is reached. Abdulla and Reddy [12] discuss the importance of thermocline shape on the packed bed performance, noting that more abrupt thermoclines increase the duration of high-quality exergy extraction, but that heat transfer processes act to reduce thermocline steepness. Zavattoni et al. [28] investigated the influence of pre-charging a packed bed on the development of thermocline stratification as steady-state operation was approached over a number of cycles and found that this could reduce the time to achieve a steady-state. Another effective approach to rapidly achieve steady-state operation is to end each charge and discharge process when the exit gas temperature reaches the required level (rather than on duration) as discussed in [15] and later in this article.

Significant work has also been undertaken in the context of CSP applications, particularly in connection with the aforementioned constraints on exit temperature variation during charge (see for example Ref. [21]). Similarly, during discharge the fluid temperature falls as the thermal front returns to the top of the packed bed, thereby affecting the steam generation process and resulting in wetter steam at the turbine inlet [8]. Zhao et al. [29] acknowledged these temperature constraints and proposed a method for determining the storage size based on acceptable exit temperature variations.

Aside from the work on single-blow and cyclic operation, some studies have considered other forms of transient behavior. For example, Bruch et al. [30] investigated rock and sand packed beds using thermal oil HTF, undertaking experiments to analyze the effect of a sudden partial-charge cycle. They found that the perturbation reduced the 'performance', which they judged on the basis of the steepness of the thermal fronts and the packed bed 'utilization' – i.e., the quantity of energy stored per cycle relative to full-charge capacity. Cyclic operation was however quickly re-established once the periodic charging cycles resumed. This is not surprising because the utilization is closely related to the duration of the charge cycle relative to the nominal charge time, although the subtle influence of exergetic losses may be difficult to determine.

Zhao et al. [31] investigated a molten-salt packed bed and also considered partial-charge cycles. They ran the packed bed to cyclic operation before subjecting it to either one, two, four or eight partial-charge cycles and then returning to regular charging durations. The greater the number of partial-charge cycles, the closer the packed bed was to establishing a new steady state. The authors noted that once the original charge cycle is resumed, less energy is stored per cycle than before the perturbations occurred – typically 1% to 3% less. However, they only undertook nine full charge cycles after the perturbation, and it is unlikely that steady-state behavior had been completely re-established. As with Ref. [30], performance quantified by the energy stored was found to be reduced by part-load cycles, but in this case the authors considered 14 days of 'practical operation' using the energy available from a CSP plant showing that partial-cycle effects would impair the performance in subsequent days.

Mertens et al. [8] investigated cyclic operation in an air-flow packed bed and described alternative operation scenarios. In one scenario, the storage is discharged to its maximum extent. In another scenario, the store is charged to a lower extent than the usual cyclic operation, although it is then discharged for the usual steady-state duration. In both scenarios, the first-law round-trip efficiency was over 100%: in cyclic operation there is a fraction of the store that is never discharged due to the thermocline slope. Some of this energy is extracted in both the alternative operation modes to provide the required duration of storage, and more energy is produced in discharge than is supplied in charge. However, the authors did not consider the influence of these alternative cycles on subsequent charge-discharge cycles.

1.3. Scope of the present work

The aim of the present article is to investigate the influence of perturbations of cycle duration on the performance of packed-bed thermal stores. An understanding of the underlying response of packed beds to perturbations is developed and provides a framework for understanding the response of packed beds to realistic load cycles.

The storage dimensions and operating temperatures have been chosen such that the packed bed would be suitable for use in a CSP plant, a PTES system, or AA-CAES. It is assumed that the mass flow rate and temperature of the inlet flow are kept constant, while only the quantity of energy available during each cycle varies. The packed bed governing equations are first described in Section 2, as well as the main exergy loss mechanisms that influence the storage performance. An overview of cyclic operation is then presented, and a theoretical explanation for the observed behavior is provided in Section 3, following which, exergetic metrics are used to offer a detailed physical explanation of the effects of perturbations to the exergy losses in Section 4. The magnitude of the response to perturbations depends on the design of the packed bed and the method of cycle control, and several options are explored. The impact of perturbations to subsequent cycles is also investigated, and of primary interest is the number of cycles required for the system to return to steady-state operation. In Sections 5 and 6, we consider the role of store segmentation and methods to reduce the performance sensitivity to charging duration perturbations. Finally, the main conclusions are given in Section 7.

2. Packed bed modelling

Thermal storage in packed beds involves several heat transfer mechanisms, including convective heat transfer between the fluid and solid, conduction along the length and radius of the store, and heat leakage from the container walls. Heat transfer between the fluid and solid results in a temperature change along the bed that is referred to as the 'thermal front', 'thermal gradient', or 'thermocline'. In an ideal reservoir with no thermal resistance between the fluid and solid, the thermal front is a step-function shape. However, dissipative processes (irreversible gas-solid heat exchange and axial conduction) lead to the thermal front spreading out during the charge-discharge process, thus affecting the storage performance.

2.1. Governing equations

The packed beds are modelled here with a modified form of the frequently-used one-dimensional Schumann equations [32,33]. The reader is referred to Refs. [15,34,35] for a derivation of the present model and numerical integration scheme. Several simplifying assumptions are made. Thermal gradients within the particles are neglected since the Biot number is small (typically ~0.07). Radial variations in temperature and flow velocity are not considered. Radial effects are predominantly due to heat leakage from the walls (which may be minimized with insulation) and variations in packing density. For instance, the void fraction increases to unity at the wall surface, leading to lower flow resistance and increased velocities but this effect is only significant within five particle diameters of the wall [36]. The stores in this investigation are sufficiently large ($D >> d_p$) that such wall effects are negligible.

The governing equations for gas temperature T_g and solid temperature T_s may be written as [15]:

$$\frac{\partial T_g}{\partial x} = \frac{T_s - T_g}{\ell} + \mathscr{C} \tag{1}$$

$$\frac{\partial T_s}{\partial t} = \frac{T_g - T_s}{\tau} + \alpha \frac{\partial^2 T_s}{\partial x^2} - \phi (T_s - T_o) \tag{2}$$

where $T_{g,s}$ is the gas/solid temperature, T_o is ambient temperature, ℓ and τ are length and time scales, α is the thermal diffusivity, ϕ is a heat leakage factor, and $\mathscr{C}$ accounts for unsteady gas accumulation. These terms are given by [15]:

$$\ell = \frac{1}{(1-\varepsilon) S_v \, \mathrm{St}} \tag{3}$$

$$\tau = \frac{\rho_s c_s}{c_p G \, S_v \, \mathrm{St}} \tag{4}$$

$$\alpha = \frac{k_{\mathrm{eff}}}{\rho_s c_s (1-\varepsilon)} \tag{5}$$

$$\phi = \frac{U_w A_w}{\rho_s c_s (1-\varepsilon) A} \tag{6}$$

$$\mathscr{C} = \frac{\varepsilon \rho_g}{G} \frac{\partial}{\partial t} \left(\frac{p}{\rho_g c_p} - T_g \right) \tag{7}$$

where ε is the void fraction, $S_v = 6/d_p$ is the particle surface-area-to-volume ratio (d_p being the diameter of an equivalent spherical particle), St is the Stanton number, ρ_s is the solid density, c_s is the solid specific heat capacity, c_p is the gas specific heat capacity, G is the mass flow rate per unit area, k_{eff} is the effective conductivity, U_w is the overall heat transfer coefficient, A_w is the wall surface area, and A is the cross-sectional area of the bed.

At typical velocities, changes in momentum flux along the store are very small, so that the pressure drop may be calculated from a simple friction-factor approach:

$$\frac{\partial p}{\partial x} = -\frac{S_v (1-\varepsilon) G^2 C_f}{2 \varepsilon^3 \rho_g} \tag{8}$$

where C_f is the friction coefficient.

Several modifications are made to this basic model, the most important of which are temperature-dependent gas and solid properties [14,15,35]. The differential equations are solved with a semi-implicit numerical scheme as described in Ref. [35] and the appendix of Ref. [15]. The derivatives are coded implicitly, with the exception of the axial conduction term in Eq. (2). Other temperature terms take the average value along the path of integration. This method allows larger time and space steps to be taken, and is shown to be significantly faster than the equivalent predictor-corrector method [35].

2.2. Exergy loss mechanisms

In order to quantify the performance of packed beds, a second-law round-trip efficiency η_{RT} of the packed bed can be defined here as the quantity of exergy that is extracted during discharge B_{dis} as a fraction of the exergy entering the store during charge, B_{chg}:

$$\eta_{\mathrm{RT}} = \frac{B_{\mathrm{dis}}}{B_{\mathrm{chg}}} = 1 - \sum \zeta \tag{9}$$

where ζ is an exergy loss coefficient. Irreversible processes, such as heat transfer across a finite temperature difference and frictional effects, lead to a reduction in the round-trip efficiency. These exergetic loss coefficients ζ are defined as

$$\zeta = \frac{T_o \, \Delta \dot{S}_{\mathrm{irr}}}{B_{\mathrm{chg}}} \tag{10}$$

where T_o is the ambient temperature, $\Delta \dot{S}_{\mathrm{irr}}$ is the irreversible entropy generation, and the inlet exergy B_{chg} is given by:

$$B_{\mathrm{chg}} = \dot{m} c_p t_{\mathrm{chg}} \left[(T_h - T_c) - T_o \ln \left(\frac{T_h}{T_c} \right) \right] = \dot{m} c_p t_{\mathrm{chg}} \beta \tag{11}$$

which depends on the mass flow rate of the heat transfer fluid (gas) $\dot{m}$, the charging duration t_{chg}, the hot inlet and cold outlet temperatures of the gas, T_h and T_c, respectively, and β represents the specific exergy.

In this study, the exergetic loss coefficients of greatest importance are the thermal losses, the pressure losses, and the exit losses, and other losses are described in more detail in Refs. [13,15,35].

The cumulative thermal loss coefficient ζ_t stems from gas-solid heat transfer $\dot{Q}$ across a finite temperature difference $T_g - T_s$, and is defined by [13]:

$$\zeta_t = \frac{T_o}{B_{\mathrm{chg}}} \int \left(\frac{1}{T_s} - \frac{1}{T_g} \right) d\dot{Q} = \frac{T_o}{\beta t_{\mathrm{chg}}} \int_0^{t_{\mathrm{chg}}} \int_0^L \frac{(T_g - T_s)^2}{T_g T_s} \frac{dx}{\ell} dt \tag{12}$$

Packed beds with longer thermal fronts tend to have lower thermal losses as the gas-solid temperature difference is lower. Increasing the area for heat transfer (by reducing the particle size, for example) also reduces thermal losses, usually at the expense of exacerbated pressure loss.

Fluid friction leads to a pressure loss coefficient ζ_p given by:

$$\zeta_p = \frac{T_o}{\beta t_{\mathrm{chg}}} \frac{\gamma - 1}{\gamma} \int_0^{t_{\mathrm{chg}}} \ln \left(\frac{p_{\mathrm{out}}}{p_{\mathrm{in}}} \right) dt \tag{13}$$

where γ is the gas ratio of specific heats and p is the pressure. It can be seen from Eqs. (12) and (13) that there is an inherent trade-off between thermal and pressure losses – for instance, as noted, increasing the heat transfer area typically leads to larger frictional losses.

The thermal front propagates along the reservoir and eventually reaches the end of the store. Since the front has a finite gradient the exit temperature increases during charge. The exit loss coefficient ζ_x due to the unrecovered exergy carried in the flow is given by:

$$\zeta_x = \frac{1}{B_{\text{chg}}} \int_0^{t_{\text{chg}}} \dot{B}(T_x, p_{\text{in}}) - \dot{B}(T_c, p_{\text{in}})\, dt \tag{14}$$

where $\dot{B}(T_x, p_{\text{in}})$ is the exergy out of the store which occurs with an exit temperature T_x and pressure equivalent to the inlet pressure (since pressure losses are already accounted for), and $\dot{B}(T_c, p_{\text{in}})$ is the exergy that would have occurred if the exit flow had the design exit temperature of T_c. Exit losses are only truly losses if the heat is rejected to the environment – it is conceivable that the heat could be used in some other process heat (or even power generation) application.

Other losses may also be modelled including the conductive loss and heat leakage from the store. The latter can be effectively controlled by the quantity of insulation and is neglected in this model. The conductive loss arises from conduction along the bed which is a dissipative process that contributes to spreading of the thermal front. This loss scales approximately with the thermal loss [15,35], but its magnitude depends on the effective conductivity k_{eff} (including radiative effects) which is a function of particle size, temperature, packing structure, flow rates, and turbulence levels. Heat leakage and conductive losses continue to occur during storage periods (i.e. between charge and discharge) but are usually small except for very long storage durations. Note that heat leakage reduces the stored (internal) energy, whilst conduction reduces only the stored exergy [37]. These losses are not considered further in this paper.

2.3. Control of packed bed charging cycles

The duration of the charge-discharge cycles has a significant effect on the efficiency and energy density of the packed bed. The simplest control system is to end charge or discharge after a given time period has elapsed. The thermal front travels with average velocity (see Ref. [13]):

$$V_f = \frac{c_p G}{(1-\varepsilon)\rho_s \bar{c}_s} = \frac{\ell}{\bar{\tau}} \tag{15}$$

where $\bar{c}_s$ is the average solid heat capacity. (Note that variations in c_s mean different parts of the thermal front move at different speeds [14]). The store thus has a nominal charging time t_N of:

$$t_N = \frac{L}{V_f} \tag{16}$$

If the charging period ends after an elapsed time t_{chg} then the dimensionless charge period Π is defined by:

$$\Pi = \frac{t_{\text{chg}}}{t_N} = \frac{t_{\text{chg}}}{\bar{\tau}} \frac{\ell}{L} \tag{17}$$

In the present work, charge and discharge durations are assumed equal. Repeatedly cycling the stores leads to steady-state periodic operation, whereby variations are identical from cycle to cycle. The steady-state charging period for a given charging duration t_{chg} is denoted here by Π^o.

The cycle durations may also be controlled by monitoring the exit temperatures and allowing them only to deviate from their design values by a prescribed amount. For example, charge of a hot store may be terminated once the quantity

$$\theta_c = \frac{T_x^{\text{chg}} - T_c}{T_h - T_c} \tag{18}$$

exceeds some specified threshold (where T_x^{chg} is the exit temperature). Similarly, the discharging period ends once the exit temperature T_x^{dis} drops by a given fraction θ_d defined by:

$$\theta_d = \frac{T_x^{\text{dis}} - T_h}{T_h - T_c} \tag{19}$$

Thermal fronts during charge and discharge are illustrated in Fig. 2 with the temperature fractions $\theta_{c,d}$ indicated. Note that controlling the thermal front in this way generally leads to much faster convergence towards a steady periodic state than fixing the charge and discharge durations.

2.4. Nominal store design

The packed bed modelled here is a hot store that is charged to 500 °C and discharged to 50 °C with air as the heat transfer fluid and magnetite as the packing material. (This is as opposed to a cold store such as that found in LAES and PTES systems, which stores exergy at sub-ambient temperatures). The store has a 'square' aspect ratio where the length and diameter are equal and a particle diameter of 20 mm, although other aspect ratios and diameters may be more optimal [5]. This storage design is therefore consistent with previous work [10,14,15]. The storage is designed to deliver 20 MW_{th} for eight hours and thus has a capacity of 160 MWh_{th}. Such a store might be considered for CSP, AA-CAES, process heat and other applications, and also operates between temperatures considered for PTES. However, results are presented in terms of non-dimensional temperatures to increase the range of applicability. Both 'simple' (i.e., unlayered) and 8-segment configurations are considered, see section 5. The nominal storage design is summarized in Table 1, and values of the major exergy loss coefficients are presented for several charging durations at cyclic operation in Table 2.

3. Cyclic operation

3.1. Transition from transient phase to steady-state cycles

When the stores are repeatedly charged and discharged with identical durations, the stores pass through a transient phase to reach steady-state operation where every cycle is identical to the one that preceded it. This is also referred to as cyclic operation. The transition takes several cycles during which the shape of the thermocline changes [8] as do the magnitude of the exergetic losses. These differences are illustrated in Fig. 3 for a packed bed where the cycle periods are controlled by fixing the durations of charge and discharge to $\Pi = 0.5$. The store is initially fully discharged, and in this case 14 cycles are required to reach steady-state operation. After the first charge cycle, the thermal front does not reach the end of the store and the exit temperature does not change. However, during discharge the exit temperature drops by 50%. This differs significantly from the steady state, where the exit temperatures at the end of charge and discharge both change by ~14% ($\theta_{c,d} = 0.14$).

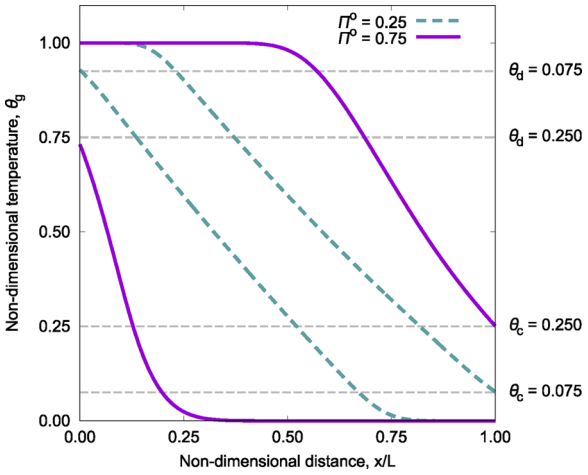


Fig. 2. Thermal fronts in a packed bed with one layer at the end of charge and discharge. Longer cycle durations lead to steeper fronts. The exit temperature controls $\theta_{c,d}$ are also illustrated.

Table 1
Design parameters of the nominal packed-bed thermal storage system.

System design	E, MWh_{th}	B_{max}, MWh_{th}	$\dot{P}$, MW_{th}	t_N, h			
Packed bed	160.0	70.0	20.0	8.0			
Working fluid	c_p, J/kg K	γ	$\dot{m}$, kg/s	R			
Air	1005	1.40	85.5	287.0			
Packing material	d_p, mm	ε	$\bar{c}_s$, J / kg K	k_{eff}, W /m K	ρ_s, kg / m^3		
Magnetite	20	0.40	874.2	1.0	5175		
Design parameters	L, m	D, m	V, m^3	T_h, °C	T_c, °C	p, bar	
	8.4	8.4	465.5	500.0	50.0	1.5	
Thermodynamic properties	ℓ, mm	τ, s	α, mm^2 / s	V_f, mm/s	St	C_f	Re
	54.7	187.1	0.368	0.293	0.10	0.475	825.1

Cyclic operation implies that the store is in the same thermodynamic state at the start of each cycle. Thus the entropy generated internally by irreversible heat exchange must be 'flushed out' of the store in order to return it to the initial conditions. This occurs via the hot exit gas which enables internal entropy generation to be balanced by the net efflux of entropy. Consequently, the cyclic thermocline shapes are quite different to those in the first cycles, as shown in Fig. 3b. In the first charging cycle, the thermal front is initially close to a step-function. Dissipative thermal processes lead to the thermal front spreading out, although the thermal front is too steep for the exit temperature to change. Over successive cycles, the thermal gradient becomes less steep, thereby allowing exergy to be rejected through the change in exit temperature.

Thermal losses during steady-state operation are lower than those in the initial cycles for two reasons. Firstly, the steep thermal fronts in the initial cycles have larger gas-solid temperature differences and reduced heat transfer area thereby leading to higher thermal losses as indicated by Eq. (12). This may be observed by considering the $(\theta_g - \theta_s)^2$ curves in Fig. 3c which effectively show the length of the profile, the integrand of which is closely related to the thermal loss. Secondly, large thermal losses occur at the transition from charge to discharge and vice versa. At the end of a charge or discharge cycle the exit temperature has changed. In the next phase, the gas flow reverses and does not equal the previous exit temperature. This temperature difference is typically larger than gas-solid temperature differences during operation, and leads to large spikes in the thermal loss that can be clearly observed in Fig. 3a. During the transient phase the temperature differences are larger than during steady-state operation.

Steady-state operation can be reached in fewer cycles by ending each cycle when a certain temperature threshold is reached, rather than after a given time period has elapsed. The thermal profiles for the first cycle and steady-state cycle are shown in Fig. 4 when the exit temperature thresholds are fixed at $\theta_{c,d} = 0.14$ (corresponding to $\Pi = 0.5$). Cyclic operation is reached after five cycles since the initial thermal fronts are very similar to the cyclic fronts. In this type of operation the duration of each cycle is different during the transient phase. For instance, to reach the required exit temperature in the first cycle requires a charging duration of $\Pi = 0.76$. System level constraints and availability of energy will determine whether this mode of operation is practicable.

3.2. Cycle period governs performance

The cycle period governs the energy density and round-trip efficiency. As expected, more exergy is stored when the charging duration is increased (see Table 2). However, Fig. 5a indicates that, at least for unlayered stores, longer charging times lead to lower round-trip efficiencies. This is partly because long charging times result in greater exit losses as the thermal front propagates further out of the store, but thermal losses also increase because the thermal front gets steeper as Π^o increases, as shown in Fig. 2 and Table 2.

In steady-state operation, the magnitudes of thermal and exit losses are inherently linked to one another through the requirement that internal irreversibilities are flushed out of the system through an increase in exit temperatures. The thermal front propagates further out of the store in longer charging cycles, this being directly linked to the steeper thermal fronts and hence greater internal losses. More exergy is thus stored at the expense of lower exergetic efficiency.

As noted, cyclic operation may also be controlled by fixing the exit temperature thresholds via θ_c and θ_d. Larger values of Π necessarily require larger $\theta_{c,d}$. These parameters may be varied independently, but once cyclic operation is reached the charge and discharge durations must be roughly equal. (This is the case if the mass flow rates and temperatures are fixed, as they are here because the returned energy must balance that absorbed during charge). Fig. 5b shows contours of round-trip efficiency obtained by varying θ_c and θ_d independently. These indicate that increasing both θ_c and θ_d generally leads to lower efficiency, but θ_c has a more significant effect on the efficiency than θ_d. (This is only true for hot stores: θ_d has the dominant effect for stores below ambient temperature [35]).

4. Perturbations to the cycle duration

Realistic load-cycles for packed-bed thermal energy storage are unlikely to follow regular charge-discharge durations due to variations in demand and the available energy supply. In this section, the impact of an erratic load-cycle is investigated. Cyclic operation with period Π^o is first established and operation is then perturbed with a single charge-discharge cycle with different period Π. Subsequent cycles are then returned to the original Π^o until the steady-state is re-established. In this section, the cycle lengths are fixed by the elapsed time, and the

Table 2
Charging durations, round-trip efficiencies and exergy loss coefficients in packed beds with several steady-state charging durations. Results are presented for stores with either one (simple) or eight segments.

		$\Pi^o = 0.25$		$\Pi^o = 0.50$		$\Pi^o = 0.75$	
		1 segment	8 segments	1 segment	8 segments	1 segment	8 segments
Charging time	h	2.0	2.0	4.0	4.0	6.0	6.0
$\theta_{c,d}$		0.075	0.055	0.14	0.13	0.25	0.25
Round-trip efficiency	%	88.4	88.4	87.6	89.5	85.8	89.2
Thermal loss coefficient	%	1.89	1.93	2.46	2.50	3.47	3.56
Pressure loss coefficient	%	9.35	8.56	9.29	7.15	9.30	5.84
Exit loss coefficient	%	0.39	1.12	0.67	0.81	1.42	1.43
Discharged exergy	MWh_{th}	15.5	15.4	30.2	30.7	43.3	45.2
Utilization	%	22.1	22.0	43.1	43.9	61.9	64.6

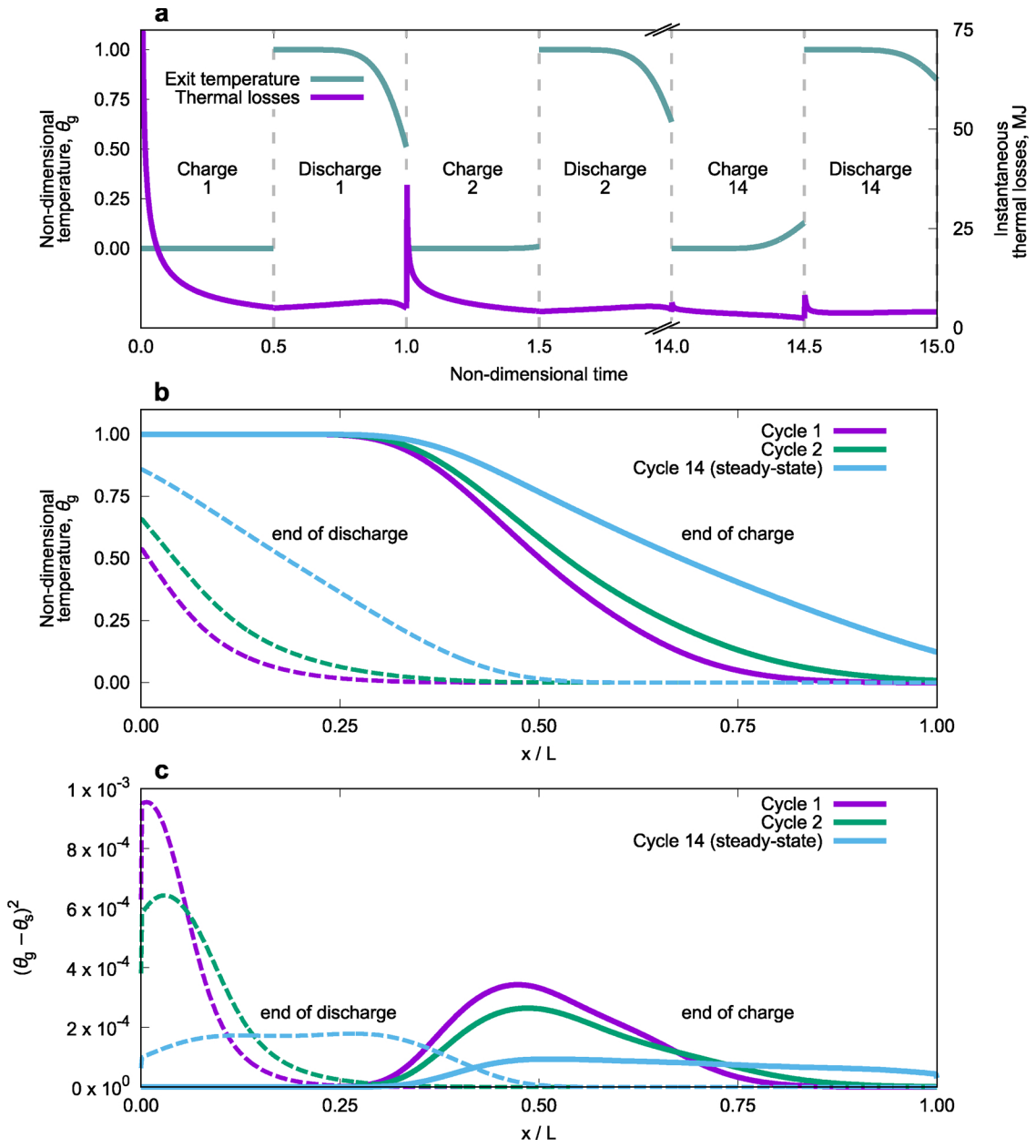


Fig. 3. Transition from transient operation to steady-state operation. Results are shown for the first two cycles and cycle 14 (steady-state) (a**)** Variation in exit temperature and instantaneous thermal losses with time. (b**)** Thermal fronts at the end of charge (right, solid) and discharge (left, dashed). (c) Gas-solid temperature difference at the end of charge (right, solid) and discharge (left, dashed).

effect of using exit temperature thresholds instead is considered in later sections.

Figs. 6 and 7 illustrate how a perturbation changes the behavior of a packed bed. Steady-state behavior is shown, as is the perturbed response, and the response of the next cycle. When the perturbation is shorter than the steady-state cycle period ($\Pi < \Pi^o$) the thermal front may not reach the end of the store during charge, so that the exit temperature does not change, see Fig. 6a. On the other hand, when $\Pi > \Pi^o$ the exit temperature increases substantially compared to the steady-state case. The perturbation not only affects the thermal front shape in that cycle, but also subsequent cycles, as shown in Fig. 7. There is consequently a 'relaxation time' as the system gradually returns to cyclic operation. By changing the thermal gradients and exit temperatures, perturbations affect the exergy losses as illustrated in Fig. 6.

The variation in total exergy loss coefficient is shown in Fig. 8a for a cycle with $\Pi^o = 0.50$ and perturbations of $\Pi = 0.25$ and 0.75. The perturbation leads to a sudden change in the total exergy loss coefficient ($\zeta_{total} = \zeta_t + \zeta_p + \zeta_x$), which eventually relaxes to the original value. Increasing the magnitude of the perturbation relative to the steady-state cycle period $|\Pi - \Pi^o|$ leads to larger changes in ζ_{total} and longer relaxation times (defined here as the number of charge-discharge cycles before ζ_t returns to within 1% of its original value).

Fig. 8b shows the relaxation times for cycles with $\Pi^o = 0.25$, 0.50 and 0.75 which are then perturbed by a single cycle with a range of Π. It is clear that relaxation times are large when Π is greater than Π^o and also when the initial Π^o is short. This is because steady-state cycles with shorter durations have lower changes in the exit temperature and reject less entropy per cycle. As a result, after a perturbation more cycles are needed for the balance between internal entropy generation and external entropy rejection to be restored. Cycles with lower Π^o also take a larger number of cycles to reach steady-state operation from a fully discharged state.

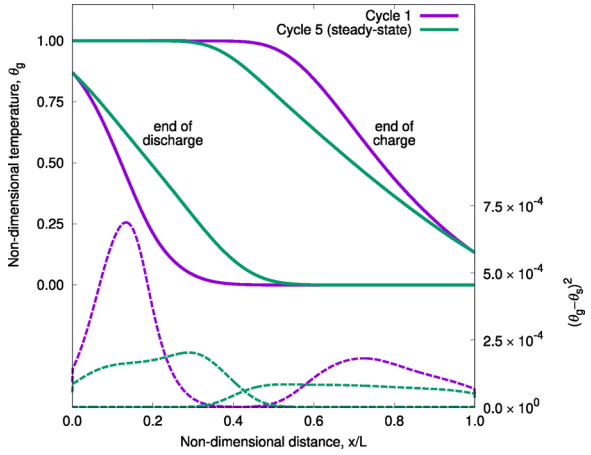


Fig. 4. Thermal fronts (solid) and gas-solid temperature difference (dashed) at the end of charge and discharge when temperature thresholds control the end of the cycle.

The percentage change in total exergy loss for steady-state cycles of $\Pi^o = 0.25$, 0.50 and 0.75 which are perturbed is shown in Fig. 9a. Perturbations with $\Pi < \Pi^o$ cause a decrease in exergy loss as the thermal front does not then reach the end of store, thereby reducing the exit loss. The converse is true for $\Pi > \Pi^o$ for which the total exergy loss increases significantly.

Thermal and pressure loss coefficients are illustrated in Fig. 9b for $\Pi^o = 0.50$. Interestingly, thermal losses are larger than the steady-state value at both small and large perturbations. A key to understanding this and some of the above observations lies in the relatively large temperature differences that exist between the gas and solid at the beginning of each charge and discharge cycle as a result of the change in exit temperature from the previous cycle. For instance, during discharge of the cycle with $\Pi^o = 0.50$, the exit temperature decreases from 500 °C to 437 °C. At the start of the next charging cycle, the inlet gas is again at 500 °C and the large temperature difference leads to relatively high thermal losses (see Eq. (12)), as shown in Fig. 6. For short perturbations, the thermal loss is lower than the steady-state value, but the exergy input is also reduced leading to increased thermal loss coefficients. For longer perturbations, the influence of the large, initial thermal losses decreases. When $\Pi > \Pi^o$ the thermal front propagates further out of the store. The large change in exit temperature leads to greater gas-solid temperature differences at the start of discharge, and thereby larger thermal losses as demonstrated in Fig. 6b.

5. Segmented packed-bed thermal stores

Segmented packed beds are stores which have been partitioned into separate layers, which may be controlled independently, as illustrated in Fig. 10. In this implementation, each segment has individual valves (with B, C, and D shut, as shown) so that the gas flow only passes through layers where significant gas-solid heat transfer occurs – i.e. within the thermal front. The flow is diverted around the remaining segments thereby reducing pressure losses. Flow is diverted into or around a segment once the gas temperature reaches a certain threshold [15]. As discussed by White et al. [15] the lower pressure loss allows smaller particles to be used, leading to a lower heat transfer loss. Segmentation was also found to reduce the dissipative conductive losses that occur during long storage periods between charge and discharge [37].

The effect of partial-charge perturbations on segmented packed beds are investigated in this section. The stores have the same geometry as in Table 1 and contain eight layers. Results are presented in Fig. 11 and are compared to beds with a single layer. Perturbations generally lead to smaller changes in total exergy loss than the unsegmented bed. This suggests that segmented stores are somewhat more robust to variable load-cycles than an unsegmented store.

Fig. 11b shows the variations in thermal, pressure and exit losses for a segmented store with perturbations for $\Pi^o = 0.50$. Notably, exit losses are larger than those of the equivalent unsegmented store for small perturbations. During charge the working fluid is input into only the first segment. The cool gas exits the segment and is diverted around the remaining segments to reduce pressure losses. As the thermal front reaches the end of the segment the exit temperature increases, and once it reaches a specified threshold (such as 1% or 5%) the gas is diverted into the next segment. Consequently, there are small exit losses from each individual segment as the front travels along the store, even for small perturbations. The exit loss magnitude at low Π could potentially be reduced by decreasing the temperature threshold at which the flow is diverted into the new segment.

In a similar way, once the thermal front has completely travelled through a segment, flow is diverted around that segment – again reducing pressure losses. As discussed in Ref. [15] this leads to additional

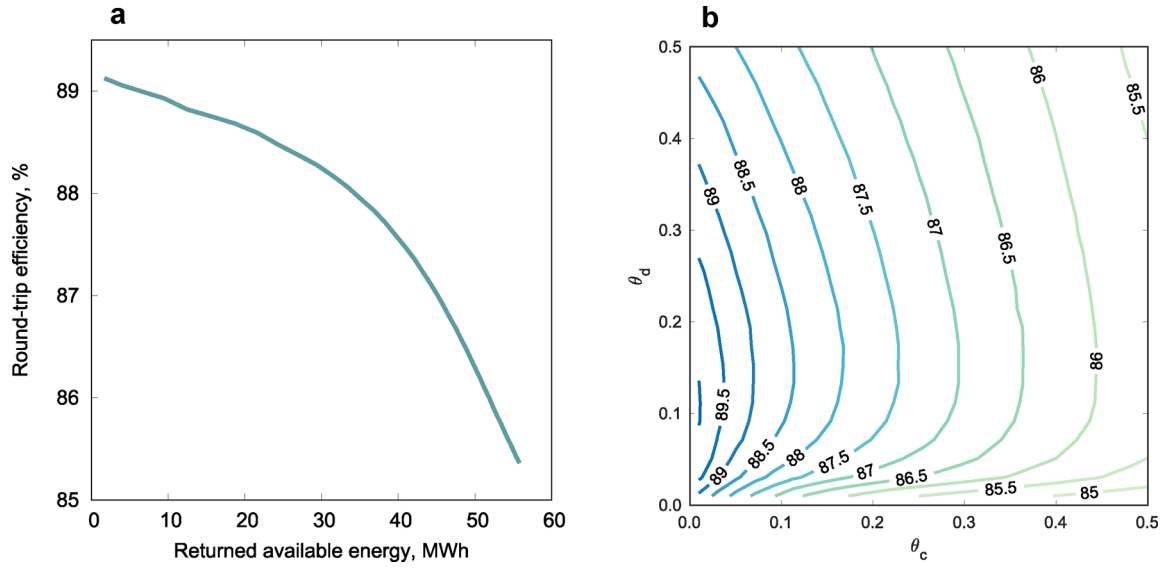


Fig. 5. Trade-off between round-trip efficiency and energy density in cyclic operation of a packed bed. (a) The trade-off illustrated for cycles controlled with cycle duration. (b) Contours of round-trip efficiency for various non-dimensional exit temperatures.

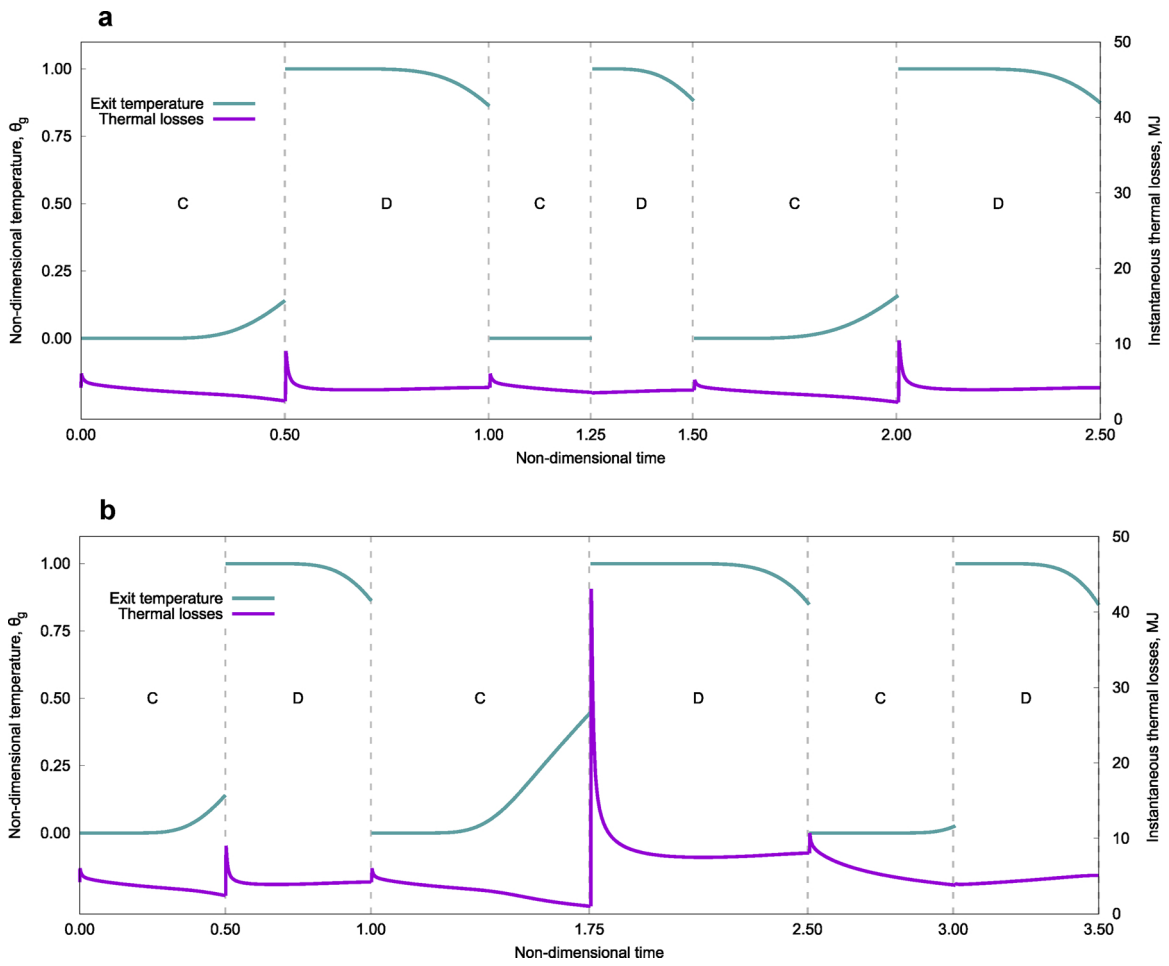


Fig. 6. Exit temperature (left-hand axis) and instantaneous thermal losses (right-hand axis) during the charge-discharge cycle preceding the perturbation, the perturbation cycle, and the following cycle. The steady-state charge period is $\Pi^o = 0.50$. (a) Perturbation duration $\Pi = 0.25$. (b) Perturbation duration $\Pi = 0.75$.

thermal losses each time a segment is switched on or off. Again, the thermal front is judged to have completely passed through a segment when the exit temperature reaches a threshold, such as 99% or 95% of $(T_h - T_c)$ at which point the flow is diverted around that segment and into the next one. There is consequently an initial temperature difference of 1% or 5% between the inlet gas and the solid temperature at the new segment inlet. This effect can be seen as the 'saw-tooth' wake in the thermal losses in Fig. 12. These additional thermal losses are reasonably

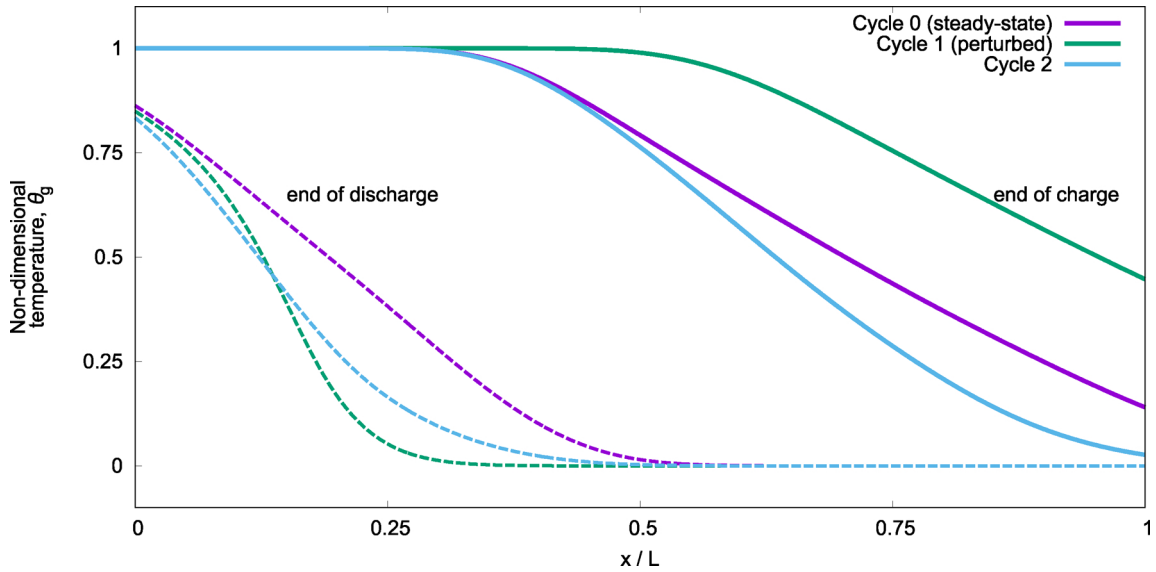


Fig. 7. Thermal fronts at the end of charge (right, solid) and end of discharge (left, dashed) for an unlayered packed bed during a steady-state cycle (cycle 0) with $\Pi^o = 0.50$, a perturbed cycle (cycle 1) with $\Pi = 0.75$, and the subsequent cycle (cycle 2) which returns to $\Pi^o = 0.50$.

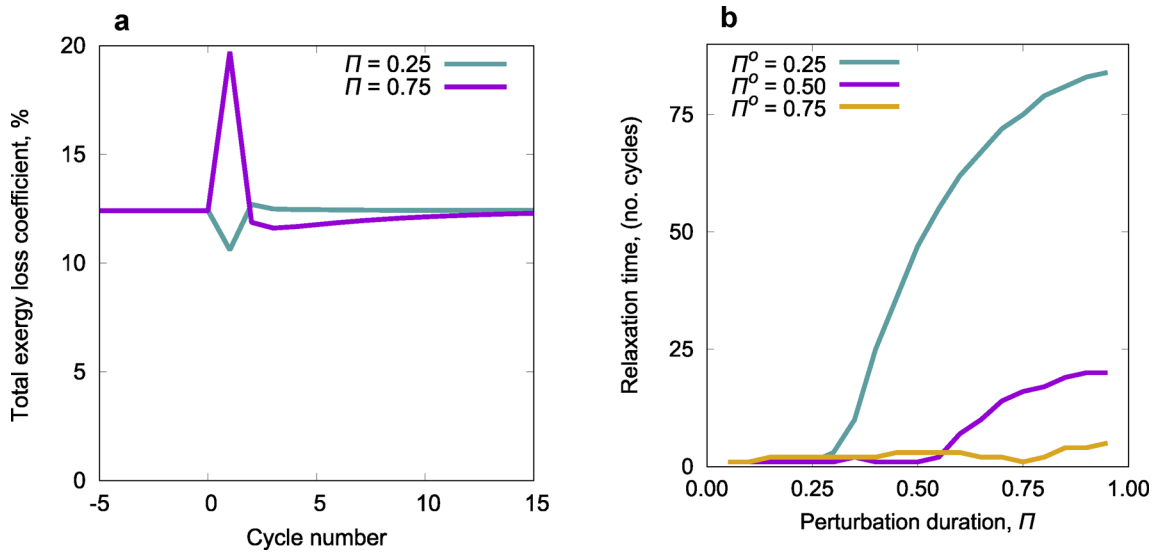


Fig. 8. Perturbing a packed bed in steady-state cyclic operation with various cycle durations. (a) The total exergy loss coefficient of each charge-discharge cycle for a packed bed with a cycle period of $\Pi^o = 0.50$ which is perturbed at cycle number 0 with periods of $\Pi = 0.25$ and 0.75. (b) The relaxation time for various perturbations for beds with cyclic periods of $\Pi^o = 0.25, 0.50, 0.75$.

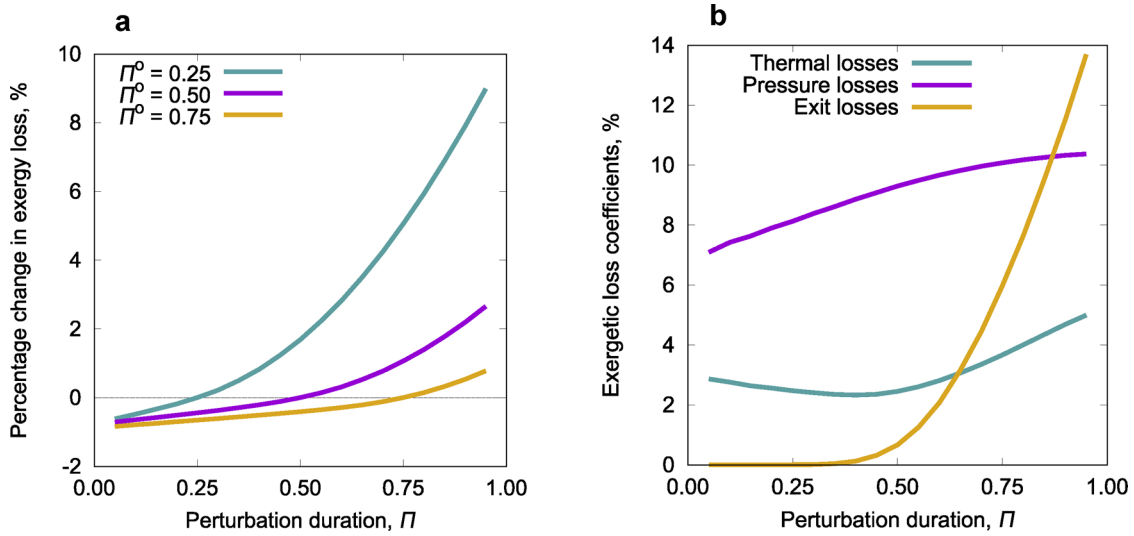


Fig. 9. (a) The effect of the perturbation magnitude on the exergy losses for packed beds with various steady-state cycle periods. (b) Effect of perturbation magnitude on exergetic loss coefficients for a packed bed with steady-state cycle period of $\Pi^o = 0.50$.

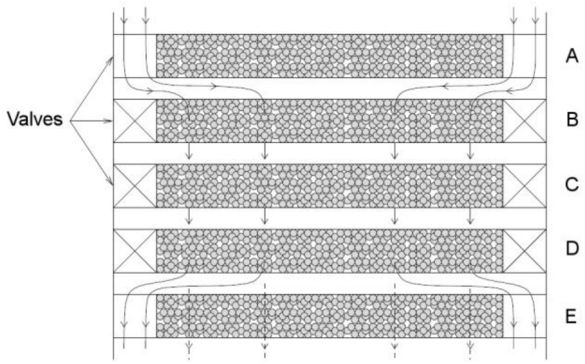


Fig. 10. Schematic of a segmented packed bed. Valves open and close to direct the gas flow through only the active layers. Valves A and E are open, and B, C and D are closed.

small, and the total thermal loss is similar to the unsegmented case.

Pressure losses for segmented stores are lower than the equivalent case in unsegmented packed beds, as a result of reduced flow through the full length of the packed bed.

6. Reducing sensitivity to perturbations

6.1. Cycle length controlled with exit temperatures

In the previous sections, cycle lengths were controlled by the duration of the charge and discharge cycle. The end of a charge or discharge phase can also be specified when the exit temperature changes by a certain fraction $\theta_{c,d}$, as defined in Eqs. (18) and (19). The acceptable change in temperature may be constrained by the system that the packed bed is integrated into.

In this section, the non-dimensional exit temperatures θ_c and θ_d are used to control the steady-state cycle duration and the perturbation magnitude. Fig. 13a indicates how perturbations affect the total exergy loss coefficients for a cycle with $\Pi^o = 0.50$ (which corresponds to

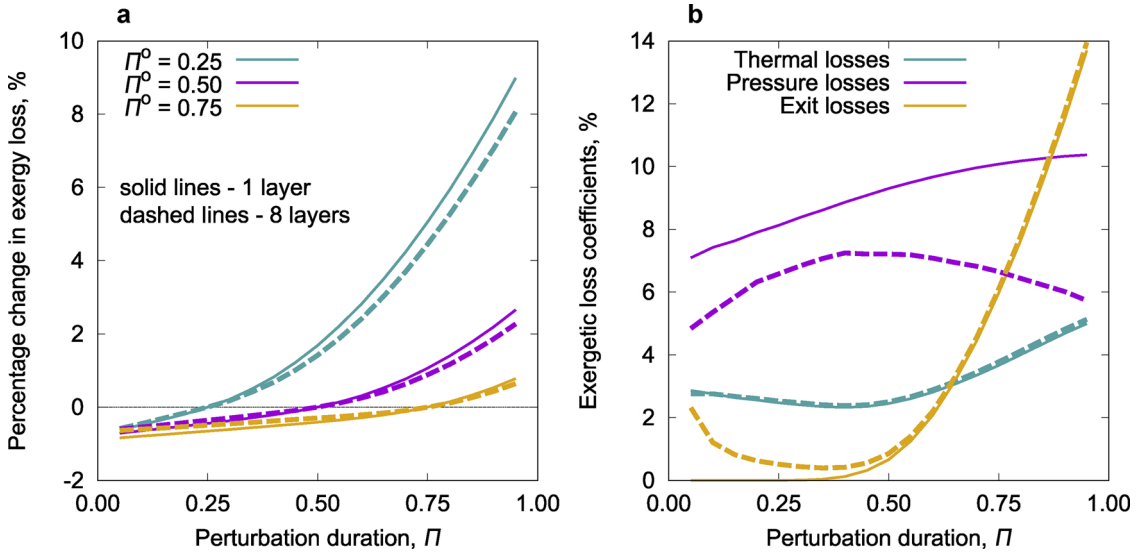


Fig. 11. Perturbation on segmented packed beds. (a) The effect of the perturbation magnitude on the exergy losses for packed beds with various steady-state cycle periods. (b) Effect of perturbation magnitude on exergetic loss coefficients for a packed bed with steady-state cycle period of $\Pi^{o} = 0.50$.

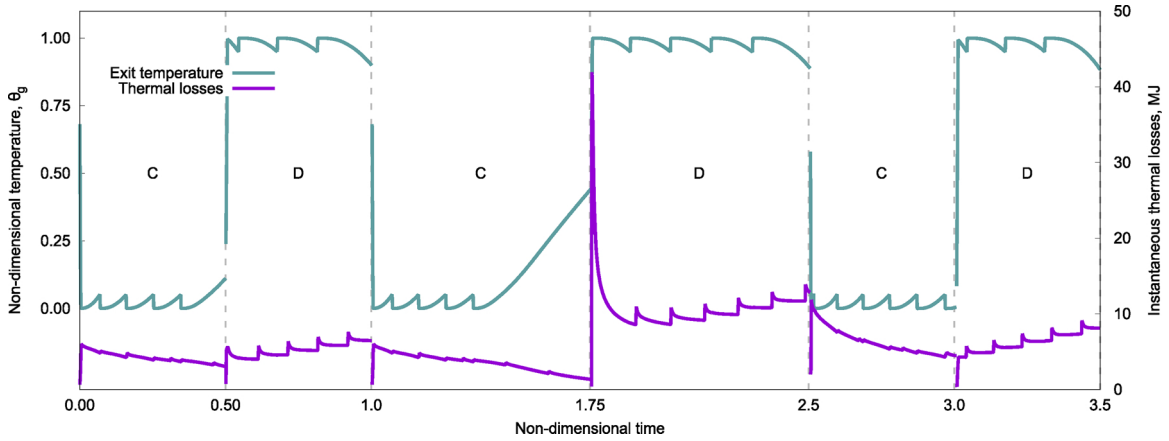


Fig. 12. Exit temperature (left-hand axis) and instantaneous thermal losses (right-hand axis) during the charge-discharge cycle preceding the perturbation, the perturbation cycle, and the following cycle. The steady-state charge period is $\Pi^{o} = 0.50$ and the perturbation duration $\Pi = 0.75$ in a packed bed with eight segments.

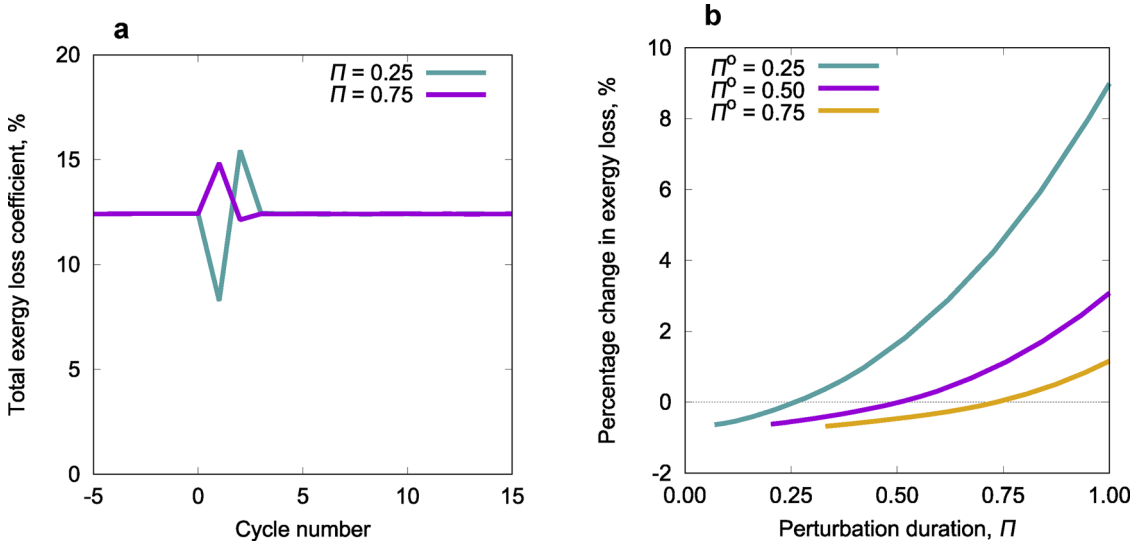


Fig. 13. Effect of perturbations on cycles that are controlled by exit temperatures $\theta_{c,d}$. (a) Total exergy loss coefficient of each cycle for a packed bed with steady-state cycle duration of $\Pi^{o} = 0.50$ and perturbations equivalent to $\Pi = 0.25, 0.75$. (b) Effect of perturbation magnitude on the total exergy losses for packed beds with steady-state cycle durations of $\Pi^{o} = 0.25, 0.50, 0.75$.

$\theta_{c,d} = 0.14$). In this case, $\theta_c = \theta_d$ so that the results are comparable with the analysis of Sections 4 and 5. The perturbations durations are equivalent to $\Pi = 0.25$ and 0.75. Notably, the relaxation time for the cycle to return to the steady-state is considerably reduced (typically one or two cycles) compared to when the cycles were controlled by cycle duration. By controlling $\theta_{c,d}$ the cycle is forced to reject a quantity of entropy that is close to the steady-state value, and the cycle therefore rapidly returns to cyclic operation. Using the exit temperatures to determine the beginning and end of a cycle is therefore an effective way to minimize the long-term effects of perturbations on cycle behavior.

The effect of the perturbation magnitude on the percentage change in total exergy losses is shown in Fig. 13b for $\Pi^o = 0.50$. As would be expected, the results show similar trends and magnitude as when the cycle duration is controlled. Small differences arise because when $\theta_{c,d}$ are controlled, the length of the charging and discharging cycles are only equal during steady-state operation. However, during perturbations, the charging cycle may have a different duration to the discharging cycle which affects the total exergy loss.

6.2. 'Realistic' control of exit temperatures

In realistic operation of packed beds, the maximum change in exit temperature is likely to be constrained by system requirements. As a result, cycles longer than the steady-state cycle duration will be unlikely. However, shorter durations may occur, as a result of fluctuations in available renewable energy, for example. When discharging the store, the exit temperature will probably always be allowed to decrease to its maximum limit, rather than setting $\theta_d = \theta_c$ as is the case in the above analysis. This will allow as much energy as possible to be discharged from the store while not exceeding system constraints.

Operating in this way leads to smaller changes in the total exergy loss coefficients than when $\theta_d = \theta_c$, particularly when $\Pi < \Pi^o$ as shown in Fig. 14. By holding θ_d at its extreme value, the discharging cycles have a duration that is similar to the steady-state value and are not a short as when $\theta_d = \theta_c$. This means that pressure and thermal losses are larger for short perturbations, and the decrease in ζ_{total} is not as significant as before.

When θ_d is fixed, the quantity of discharged exergy also differs compared to when $\theta_d = \theta_c$ as shown in Fig. 15. As would be expected when $\Pi < \Pi^o$ the discharged exergy is greater for fixed θ_d than when the exit temperature fractions are equal. The opposite result is observed when $\Pi > \Pi^o$. These results indicate that on days when less energy is available, it is preferable to discharge the store to the maximum θ_d as this provides a quantity of exergy more similar to the steady-state value.

Controlling cycle durations by setting limits on the exit temperatures is an effective way to minimize the long-term effect of perturbations and enable more consistent and robust operation of the stores.

7. Conclusions

Packed beds can provide thermal storage services in a range of applications, and in particular may address the intermittent generation of renewable power systems. Previous studies of packed beds typically concentrate on the first charging cycles, or on steady-state cyclic operation. However, when integrated into a renewable energy system packed beds may be charged or discharged with different quantities of energy each day. In this article, packed beds are operated until cyclic operation is reached, and the charging duration is then perturbed with either shorter or longer cycles. An understanding of the underlying response of packed beds to perturbations is therefore developed. Future work will investigate the response to realistic load-cycles, and this initial study provides the framework for understanding the packed bed response.

A rock-filled air-flow packed bed operating between 500 °C and 50 °C is considered. Stores of this type are suitable for several applications, and the results of this work may be generalized to systems such as CSP, PTES, and AA-CAES.

Steady-state operation whereby each cycle is identical to the previous cycle is first considered. To reach cyclic operation, a transient phase is passed through during which a balance is established between the entropy rejected at the exit of the store and the internal entropy generated by irreversibilities within the store. This balance leads to a trade-off between efficiency and energy density: longer duration cycles store greater quantities of exergy at the expense of round-trip efficiency. For instance, for the store considered here increasing the cycle period from $\Pi = 0.25$ to 0.75 led to a reduction in efficiency from 88.4% to 85.8% and an increase in discharged exergy from 15.5 MWh_{th} to 43.3 MWh_{th}.

The impact of perturbations to the cycle length is then investigated, and the results are found to be predominantly influenced by exergy losses as the thermal front exits the store. If the perturbation duration is shorter than the steady-state cycle period, then total exergy losses decrease since exit losses are lower. On the other hand, longer perturbations lead to an increase in exergy losses. The change in exergy loss is influenced by the magnitude of the perturbation, the direction of the perturbation, and the steady-state cycle duration. Perturbations longer and of a greater difference to the steady-state cycle duration lead to larger changes in the total exergy loss. For instance, in one case considered here, the exergy losses in a cycle with period $\Pi = 0.5$ which is perturbed by a $\Pi = 0.75$ cycle increased by 8%, while a perturbation of period $\Pi = 0.25$ reduced the total losses by 2%.

Perturbations also affect subsequent cycles, and several cycles may be required before steady-state operation is once again achieved. This relaxation time is typically fewer than five cycles if the perturbation was shorter than the steady-state cycle period. However, longer perturbations could lead to relaxation times of 10–50 cycles. Furthermore, the shorter the steady-state cycle period the longer the cycle takes to return to steady-state behavior after the perturbation.

Packed beds which have been segmented into layers are considered, and it is found that perturbations typically have a less significant effect on exergy losses than in unsegmented stores. Furthermore, segmentation reduces pressure losses by 1–4 % for the stores considered here, although exit losses may increase due to the mechanism of turning individual layers on and off.

The end of the charging and discharging cycles may be controlled by either the duration of the cycles, or by the change in exit temperatures. Fixing exit temperatures is likely to be a more realistic operating scenario due to constraints imposed by the wider system. In this case, it is found that perturbations have a reduced effect on changes in total

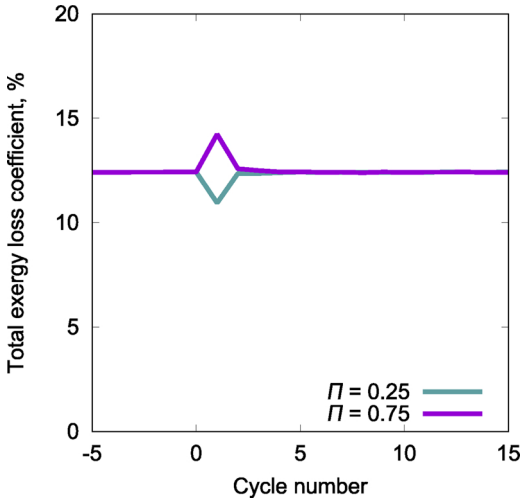


Fig. 14. Effect of perturbations on the total exergy loss coefficients of a cycle with steady-state cycles of $\Pi^o = 0.50$ with the discharging exit temperature fraction fixed at $\theta_d = 0.14$.

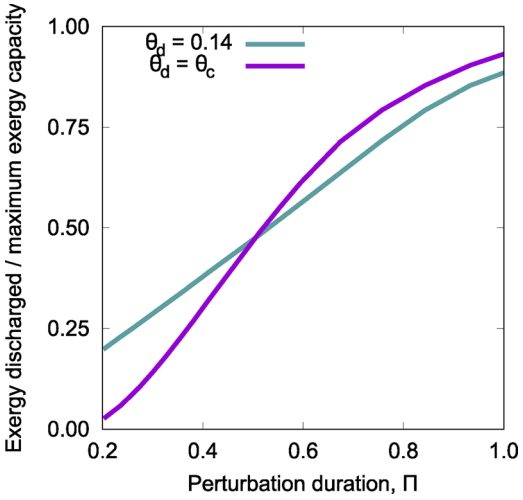


Fig. 15. Normalized discharged exergy in the perturbed cycle. $\Pi^{o} = 0.50$ which corresponds to $\theta_{c,d} = 0.14$. In one case the exit temperatures in charge and discharge of the perturbed cycle are equal, $\theta_d = \theta_c$ and in the other case, the perturbed θ_d is fixed to the steady-state value ($\theta_d = 0.14$).

exergy loss. Furthermore, the time taken to re-establish steady-state operation is reduced to only one or two charge-discharge cycles. It is also found that always discharging the store to its maximum extent increases the exergy that is extracted, and reduces changes in storage behavior.

It is debatable whether exit losses count as exergy losses, as the exergy does not necessarily need to be rejected but could be used in other applications. Since thermal losses follow the same trends as exit losses, the behavior described in this article is valid whether or not exit losses are included. However, the magnitude of changes in the total exergy loss would be reduced if exit losses were neglected.

These results inform operation of packed beds in real operating scenarios. Packed beds are more resilient to changes in available energy if the store is not suddenly over-charged (i.e. longer perturbations), and if the steady-state cycle duration is relatively long. Furthermore, ending charge or discharge cycles when a certain exit temperature is reached reduces the impact of perturbations in the store performance, and the performance of subsequent cycles.

Acknowledgements

This work was supported by the UK Engineering and Physical Sciences Research Council (EPSRC) [grant numbers EP/J006246/1, EP/J006041/1, and EP/P004709/1]. The authors gratefully acknowledge this support.

This work was authored, in part, by the National Renewable Energy Laboratory, operated by Alliance for Sustainable Energy, LLC, for the U.S. Department of Energy (DOE). The views expressed in the article do not necessarily represent the views of the DOE or the U.S. Government. The U.S. Government retains and the publisher, by accepting the article for publication, acknowledges that the U.S. Government retains a nonexclusive, paid-up, irrevocable, worldwide license to publish or reproduce the published form of this work, or allow others to do so, for U.S. Government purposes.

References

[1] E. Barbour, D. Mignard, Y. Ding, Y. Li, Adiabatic Compressed Air Energy Storage with packed bed thermal energy storage, Appl. Energy 155 (2015) 804–815, https://doi.org/10.1016/j.apenergy.2015.06.019.

[2] S. Zavattoni, M. Barbato, Pilot-scale demonstration of advanced adiabatic compressed air energy storage, Part 1 : Plant description and tests with thermal-energy storage, J. Energy Storage. 17 (2018) 129–139, https://doi.org/10.1016/j.est.2018.02.004.

[3] R. Morgan, S. Nelmes, E. Gibson, G. Brett, Liquid air energy storage – analysis and first results from a pilot scale demonstration plant, Appl. Energy 137 (2015) 845–853, https://doi.org/10.1016/j.apenergy.2014.07.109.

[4] A. White, G. Parks, C.N. Markides, Thermodynamic analysis of pumped thermal electricity storage, Appl. Therm. Eng. 53 (2013) 291–298, https://doi.org/10.1016/j.applthermaleng.2012.03.030.

[5] J.D. McTigue, A.J. White, C.N. Markides, Parametric studies and optimisation of pumped thermal electricity storage, Appl. Energy 137 (2015) 800–811, https://doi.org/10.1016/j.apenergy.2014.08.039.

[6] M. Mercangöz, J. Hemrle, L. Kaufmann, A. Z'Graggen, C. Ohler, Electrothermal energy storage with transcritical CO2 cycles, Energy 45 (2012) 407–415, https://doi.org/10.1016/j.energy.2012.03.013.

[7] P.A. Galione, C.D. Pérez-segarra, I. Rodríguez, A. Oliva, J. Rigola, Multi-layered solid-PCM thermocline thermal storage concept for CSP plants. Numerical analysis and perspectives, Appl. Energy 142 (2015) 337–351, https://doi.org/10.1016/j.apenergy.2014.12.084.

[8] N. Mertens, F. Alobaid, L. Frigge, B. Epple, Dynamic simulation of integrated rock-bed thermocline storage for concentrated solar power, Sol. Energy 110 (2014) 830–842, https://doi.org/10.1016/j.solener.2014.10.021.

[9] R. Anderson, L. Bates, E. Johnson, J.F. Morris, Packed bed thermal energy storage : A simplified experimentally validated model, J. Energy Storage 4 (2015) 14–23, https://doi.org/10.1016/j.est.2015.08.007.

[10] J. McTigue, A. White, A comparison of radial-flow and axial-flow packed beds for thermal energy storage, Appl. Energy (2017), https://doi.org/10.1016/j.apenergy.2017.08.179.

[11] A. Bruch, J.F. Fourmigué, R. Couturier, Experimental and numerical investigation of a pilot-scale thermal oil packed bed thermal storage system for CSP power plant, Sol. Energy 105 (2014) 116–125, https://doi.org/10.1016/j.solener.2014.03.019.

[12] A. Abdulla, K.S. Reddy, Effect of operating parameters on thermal performance of molten salt packed-bed thermocline thermal energy storage system for concentrating solar power plants, Int. J. Therm. Sci. 121 (2017) 30–44, https://doi.org/10.1016/j.ijthermalsci.2017.07.004.

[13] A.J. White, Loss analysis of thermal reservoirs for electrical energy storage schemes, Appl. Energy 88 (2011) 4150–4159, https://doi.org/10.1016/j.apenergy.2011.04.030.

[14] A. White, J. McTigue, C. Markides, Wave propagation and thermodynamic losses in packed-bed thermal reservoirs for energy storage, Appl. Energy 130 (2014) 648–657, https://doi.org/10.1016/j.apenergy.2014.02.071.

[15] A.J. White, J.D. McTigue, C.N. Markides, Analysis and optimisation of packed-bed thermal reservoirs for electricity storage applications, Proc. Inst. Mech. Eng. Part A J. Power Energy 230 (2016) 739–754.

[16] D.M. Crandall, E.F. Thacher, Segmented thermal storage, Sol. Energy 77 (2004) 435–440, https://doi.org/10.1016/j.solener.2003.08.011.

[17] M. Li, Y. Qiu, M. Li, Cyclic thermal performance analysis of a traditional single-layered and of a novel multi-layered packed-bed molten salt thermocline tank, Renew. Energy 118 (2018) 565–578, https://doi.org/10.1016/j.renene.2017.11.038.

[18] G. Zanganeh, A. Pedretti, S. Zavattoni, M. Barbato, A. Steinfeld, Packed-bed thermal storage for concentrated solar power – pilot-scale demonstration and industrial-scale design, Sol. Energy 86 (2012) 3084–3098, https://doi.org/10.1016/j.solener.2012.07.019.

[19] J. Marti, L. Geissbühler, V. Becattini, A. Haselbacher, A. Steinfeld, Constrained multi-objective optimization of thermocline packed-bed thermal-energy storage, Appl. Energy 216 (2018) 694–708, https://doi.org/10.1016/j.apenergy.2017.12.072.

[20] R. Daschner, S. Binder, M. Mocker, Pebble bed regenerator and storage system for high temperature use, Appl. Energy 109 (2013) 394–401, https://doi.org/10.1016/j.apenergy.2012.10.062.

[21] T. Fasquelle, Q. Falcoz, P. Neveu, J. Ho, A temperature threshold evaluation for thermocline energy storage in concentrated solar power plants, J. Appl. Energy 212 (2018) 1153–1164, https://doi.org/10.1016/j.apenergy.2017.12.105.

[22] G. Zanganeh, R. Khanna, C. Walser, A. Pedretti, A. Haselbacher, A. Steinfeld, Experimental and numerical investigation of combined sensible–latent heat for thermal energy storage at 575°C and above, Sol. Energy 114 (2015) 77–90, https://doi.org/10.1016/j.solener.2015.01.022.

[23] Z. Liao, G. Zhao, C. Xu, C. Yang, Y. Jin, X. Ju, X. Du, Efficiency analyses of high temperature thermal energy storage systems of rocks only and rock-PCM capsule combination, Sol. Energy 162 (2018) 153–164, https://doi.org/10.1016/j.solener.2017.12.065.

[24] E.A. Abdel-Ghaffar, Steady Periodic Heat Transfer in a Rock Bed Exposed to Sinusoidal Air Temperature Variation, PhD Thesis Iowa State University, 1980.

[25] P.-C. Lu, T.-L. Hon, Single-phase response of a packed-bed thermal storage unit to a general variation in the rate of through-flow, Alternative Energy Sources: Proceedings of the Miami International Conference on Alternative Energy Volume 1, (1983), pp. 209–232.

[26] D.E. Beasley, J.A. Clark, Transient response of a packed bed for thermal energy storage, Int. J. Heat Mass Transf. 21 (1984) 1659–1669.

[27] T. Esence, R. Bayón, A. Bruch, E. Rojas, Study of thermocline development inside a dual-media storage tank at the beginning of dynamic processes, AIP Conference Proceedings 1850, 080009 (2017), https://doi.org/10.1063/1.4984430.

[28] S.A. Zavattoni, M.C. Barbato, G. Zanganeh, A. Pedretti, High temperature thermocline TES - Effect of system pre-charging on thermal stratification, AIP Conf. Proc. 1734 (2016), https://doi.org/10.1063/1.4949141.

[29] B. Zhao, M. Cheng, C. Liu, Z. Dai, An efficient tank size estimation strategy for packed-bed thermocline thermal energy storage systems for concentrated solar power, Sol. Energy 153 (2017) 104–114, https://doi.org/10.1016/j.solener.2017.

05.057.
[30] A. Bruch, S. Molina, T. Esence, J.F. Fourmigue, R. Couturier, Experimental investigation of cycling behaviour of pilot-scale thermal oil packed-bed thermal storage system, Renew. Energy 103 (2017) 277–285, https://doi.org/10.1016/j.renene.2016.11.029.
[31] B. Zhao, M. Cheng, C. Liu, Z. Dai, Cyclic thermal characterization of a molten-salt packed-bed thermal energy storage for concentrating solar power, Appl. Energy 195 (2017) 761–773, https://doi.org/10.1016/j.apenergy.2017.03.110.
[32] T.E.W. Schumann, Heat transfer: a liquid flowing through a porous prism, J. Franklin Inst. 208 (1929) 405–416, https://doi.org/10.1016/S0016-0032(29)91186-8.
[33] A. Anzelius, Heating by means of percolating media (in German), J. Appl. Math. Mech. 6 (1926), https://doi.org/10.1002/zamm.19260060404.
[34] A. Willmot, Dynamics of Regenerative Heat Transfer, Taylor & Francis, 2002.
[35] J. McTigue, Analysis and Optimisation of Thermal Energy Storage, PhD Thesis, University of Cambridge, 2016, https://doi.org/10.17863/CAM.7084.
[36] W. van Antwerpen, C.G. du Toit, P.G. Rousseau, A review of correlations to model the packing structure and effective thermal conductivity in packed beds of mono-sized spherical particles, Nucl. Eng. Des. 240 (2010) 1803–1818, https://doi.org/10.1016/j.nucengdes.2010.03.009.
[37] J.D. McTigue, A.J. White, Segmented packed beds for improved thermal energy storage performance, IET Renew. Power Gener. 10 (2016) 1498–1505, https://doi.org/10.1049/iet-rpg.2016.0031.